Water Air Soil Pollut (2022) 233: 375
https://doi.org/10.1007/s11270-022-05847-8

# Differentiating and Quantifying Carbonaceous (Tire, Bitumen, and Road Marking Wear) and Non-carbonaceous (Metals, Minerals, and Glass Beads) Non-exhaust Particles in Road Dust Samples from a Traffic Environment

**Ida Järlskog · David Jaramillo-Vogel · Juanita Rausch · Sébastien Perseguers · Mats Gustafsson · Ann-Margret Strömvall · Yvonne Andersson-Sköld**

Received: 17 May 2022 / Accepted: 24 August 2022 / Published online: 5 September 2022


**Abstract** Tires, bitumen, and road markings are important sources of traffic-derived carbonaceous wear particles and microplastic (MP) pollution. In this study, we further developed a machine-learning algorithm coupled to an automated scanning electron microscopy/energy dispersive X-ray spectroscopy (SEM/EDX) analytical approach to classify and quantify the relative number of the following subclasses contained in environmental road dust: tire wear particles (TWP), bitumen wear particles (BiWP), road markings, reflecting glass beads, metallics, minerals, and biogenic/organics. The method is non-destructive, rapid, repeatable, and enables information about the size, shape, and elemental composition of particles 2–125 µm. The results showed that the method enabled differentiation between TWP and BiWP for particles > 20 µm with satisfying results. Furthermore, the relative number concentration of the subclasses was similar in both analyzed size fractions (2–20 µm and 20–125 µm), with minerals as the most dominant subclass (2–20 µm $\bar{x}$ = 78%, 20–125 µm $\bar{x}$ = 74%) followed by tire and bitumen wear particles, TBiWP, (2–20 µm $\bar{x}$ = 19%, 20–125 µm $\bar{x}$ = 22%). Road marking wear, glass beads, and metal wear contributed to $\bar{x}$ = 1%, $\bar{x}$ = 0.1%, and $\bar{x}$ = 1% in the 2–20-µm fraction and to $\bar{x}$ = 0.5%, $\bar{x}$ = 0.2%, and $\bar{x}$ = 0.4% in the 20–125-µm fraction. The present results show that road dust appreciably consists of TWP and BiWP within both the coarse and the fine size fraction. The study delivers quantitative evidence of the importance of tires, bitumen, road marking, and glass beads besides minerals and metals to wear particles and MP pollution in traffic environments based on environmental (real-world) samples

**Supplementary Information** The online version contains supplementary material available at https://doi.org/10.1007/s11270-022-05847-8.

I. Järlskog (✉) · M. Gustafsson · Y. Andersson-Sköld
Swedish National Road and Transport Research Institute (VTI), 581 95 Linköping, Sweden
e-mail: ida.jarlskog@vti.se

I. Järlskog · Y. Andersson-Sköld
Department of Architecture and Civil Engineering, Division of Geology and Geotechnics, Chalmers University of Technology, 412 96 Gothenburg, Sweden

D. Jaramillo-Vogel · J. Rausch
Particle Vision Ltd, Passage du Cardinal 13B, 1700 Fribourg, Switzerland

S. Perseguers
Gradiom Sàrl, Avenue de Tivoli 4, 1700 Fribourg, Switzerland

A.-M. Strömvall
Department of Architecture and Civil Engineering, Division of Water Environment Technology, Chalmers University of Technology, 412 96 Gothenburg, Sweden

**Keywords** Tire wear particles · Automated single-particle SEM/EDX analysis · Machine learning · Road dust differentiation · TRWP · Field samples

## 1 Introduction

Traffic-derived non-exhaust particles, e.g., wear and tear from tires, brakes, vehicle bodies, and roads, are an important source of air, soil, and road runoff pollution. The weight and number of vehicles are increasing worldwide, resulting in higher emissions of non-exhaust particles. Therefore, the non-exhaust emissions are predicted to increase, even if the vehicle fleet is transformed from combustion engines to electric within the near future (Beddows & Harrison, 2021). Non-exhaust particles are directly emitted to the road where the particles can deposit and accumulate on the road surface or in the nearby area. The particles can also be further transported through the air reaching more distal environments, e.g., soils and multiple surfaces, (Magnusson et al., 2020), via road runoff to the stormwater systems (Järlskog et al., 2020, 2021) and farther to receiving waters (Bondelind et al., 2019). Non-exhaust particles accumulated as road dust on the road surface can also be suspended in the air by traffic and/or wind or transported in splash and spray from vehicles during wet conditions (Gustafsson et al., 2019). Traffic-derived non-exhaust particles contain numerous pollutants such as metals, organic compounds, and microplastics (MP), and are often found in the environment with encrustations of minerals or as mixtures with other particles (Abbasi et al., 2017; Järlskog et al., 2021; Panko et al., 2012; Rausch et al., 2022).

Brake wear particles and tire wear particles (TWP) have previously been identified as major sources of metal pollution in the traffic environment since they can contain high amounts of copper (Cu), lead (Pb), and zinc (Zn) (Degaffe & Turner, 2011; Ma et al., 2021; Müller et al., 2020). Zinc can also be found in galvanized steel such as crash barriers and lampposts. Furthermore, nickel (Ni), chromium (Cr), and Pb can be released from the vehicles during driving, e.g., by engine wear or metal plating. Brake wear particles are formed due to the mechanical interaction between the brake caliper and rotor during braking (Wahlström et al., 2009) and the release of metals is also dependent on driving behavior and the traffic environment (Folkeson, 2005; Hjortenkrans et al., 2007). Thermal processes at higher temperatures, related to hard or frequent braking, result in high emissions of ultrafine particles (Nosko & Olofsson, 2017; Vojtíšek-Lom et al., 2021). Emissions also depend on vehicle weight, where heavier cars emit more brake wear particles at similar deceleration rates (Oroumiyeh & Zhu, 2021).

Bitumen wear particles (BiWP) are also commonly found in environmental samples. Bitumen is a crude oil derivative and contains, besides carbon and oxygen, elements like sulfur, nitrogen, vanadium, nickel, and calcium in low concentrations (Holý & Remišová, 2019). Bitumen is used in the wearing course and the binder layers of the pavement, which contains also variable but usually high proportions of minerals. Therefore, it is common to find bitumen sticking to mineral grains and forming particle agglomerates by its adhesive properties.

Tire wear particles are generated when the tire tread interacts with the road surface during motion, especially during slip, i.e., while accelerating, deaccelerating, and/or steering (Baensch-Baltruschat et al., 2020). The generation is also influenced by the characteristics of the tire, the size and weight of the vehicle, the pavement, and the driving behavior and conditions, e.g., deviations in wheel alignment and tire inflation pressure (Kole et al., 2017; Verschoor et al., 2016; Wagner et al., 2018). TWP has been defined as one of the major sources of MP (Kole et al., 2017). In the environment, TWP are found as encrustations with minerals or bitumen called tire and road wear particles, TRWP. However, compared to traditional MP, TWP and TRWP have been less studied, and the particles are more difficult to analyze, due to their complex composition and black color. The presence of carbon black causes a disruptive fluorescence phenomenon when exposed to laser lights, resulting in almost complete absorption of the infrared light (Eisentraut et al., 2018; Kole et al., 2017). Several studies have been published recently using pyrolysis GC/MS for the quantification of specific tracers present in TWP (ISO, 2017a, b; Goßmann et al., 2021; Parker-Jurd et al., 2021; Rødland et al., 2022a), but a standardized method for sampling, sample preparation, and analysis is still missing (Lusher et al., 2021; Rauert et al., 2021). This is mainly due to the difficulties of recognizing TWP in environmental samples and that analytical

methods are either affected by time-consuming sample preparations or limited to specific size ranges (Jekel, 2019).

In a recent study, scanning electron microscope energy dispersive X-ray analysis (SEM/EDX) was used in combination with time-of-flight secondary ion mass spectrometry (ToF–SIMS) for chemical mapping of TRWP (Kovochich et al., 2021). The authors showed promising results and identified TRWP (6−120 µm) based on shape (elongated/round) and chemical composition, but the method required an extensive sample preparation prior to analysis, and the identification of TWP was not automated. Recently, a new approach combining automated SEM/EDX single-particle analysis with a machine learning-based (ML) classification algorithm for differentiation and quantification of the most dominant particles in urban air samples (including TWP and non-exhaust particles) was presented (Rausch et al., 2022). The identification and differentiation of the single-particle subclasses and their proportions were based on elemental composition combined with morphological and textural properties. The method delivered information about mass and number concentration combined with size, shape, composition, and textural heterogeneity of single particles.

In this paper, the automated SEM/EDX/ML-based method was further developed by including new subclasses expected in road dust samples. The aim of this study was to develop a rapid and repeatable method to differentiate between and within carbonaceous traffic-derived wear particles like TWP, BiWP, and road marking wear and non-carbonaceous non-exhaust particles like minerals, metals, and glass beads in road dust samples, including a specifically designed sample preparation and the application of the complete method to a case study. To our best knowledge, this is the first study differentiating and quantifying this wide spectrum of traffic-derived wear particles in road dust samples. Moreover, it provides additional information about elemental composition, shape, size, and particle surface/texture as the result of one single, and automated analysis.

## 2 Method

This is a method development study for traffic-derived wear particles collected in the environment. Figure 1 shows a schematic illustration of the method set-up: samples were collected on the road surface, analyzed with an automated SEM/EDX single-particle analysis, thereafter, classified into different subclasses with ML, and the relations between different subclasses are presented as relative number concentrations, e.g., with a pie chart.

### 2.1 Field Sampling

Road dust samples were collected at Testsite E18, a national research station located on the highway between Västerås and Enköping, Sweden (Figure S7). The annual average daily traffic (AADT) is approximately 11,000 vehicles, and the speed limit is 120 km/h. To the date of the sampling, the pavement at Testsite E18 consisted of a stone mastic asphalt with a maximum gravel size of 11 mm (SMA11); the binder is a polymer modified bitumen. Samples were collected adjacent to the kerb in all seasons, on a total of five occasions between 2018 and 2020. Road dust samples were collected from the road surface with a wet dust sampler II (WDS II) as previously described in (Gustafsson et al., 2019; Jonsson et al., 2008; Lundberg et al., 2019). The sampling technique is automated, and 340 mL of high pressurized de-ionized water is used to clean a standardized, circular area of the road surface (20.42 $cm^2$) whereafter the road dust-water mixture is transferred into a glass bottle by compressed air. Each bottle contains a composite sample, where three sub-samples of 340 mL have been pooled together by moving the WDS II approximately 20 cm in the driving direction between every sample. This step was performed to maximize the sampling area ensuring sampling on a previously unsampled area of the road surface and, hence, to reduce the risk of extreme values.

### 2.2 Sample Preparation

From each sample bottle, containing 1L of road dust-water mixture:

- 200 mL was analyzed for particle size distribution by laser diffraction (see 2.2.1)
- Approximately 500 mL was used for the gravimetric analysis (see 2.2.1).

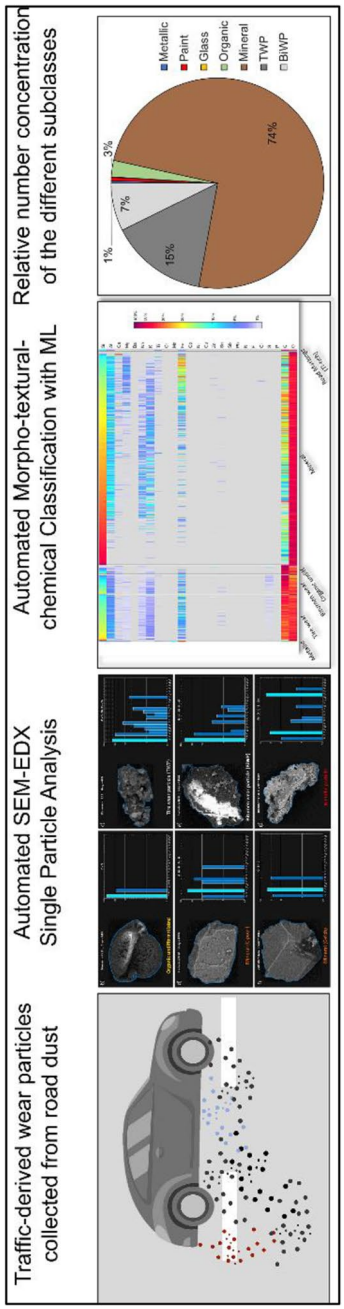


**Fig. 1** Schematic illustration of sampling, analysis, particle classification, and an example of the results

- 300 mL were sieved using mesh sizes 125 µm and 20 µm (for further details see 2.2.2). The sieved fractions were used for single-particle analysis.

### *2.2.1 Grainsize and Gravimetric Analysis*

The road dust samples were analyzed for particle size distribution using a laser granulometer (Mastersizer 3000 from Malvern Panalytical) and the Mie scattering model. Due to the upper size limit (2 mm) of the laser granulometer, all samples were pre-sieved over an ISO 3310 VWR® 12″ (mesh size 2 mm). The refraction index was based on earlier measurement experiences (Gustafsson et al., 2019) and the measurements were performed in triplicates (Supplementary material, 2.1). For the gravimetric analysis, 500 mL was filtered through a pre-weighted Munktell 00H filter (particle retention 1−2 µm). After drying, the filters were conditioned in an exicator and weighed whereafter the particle mass concentration was calculated (g/L). The total amount of road dust ($g/m^2$) was calculated based on the information from the gravimetric analysis and the area of the WDS II sample by assuming that the road dust was evenly distributed on the road surface.

### *2.2.2 Preparation for Single-Particle Analysis*

The road dust samples were separated into different particle size fractions. Approximately 300 mL was wet sieved with tap water in sequence through 125-µm and 20-µm mesh sieves (VWR® test sieves, ISO 3310) with the use of a showerhead and a shake-table. The fraction > 125 µm was separated but not further analyzed in the present study as it was included in previous studies performed by the authors of this publication (Järlskog et al., 2020 and Järlskog et al., 2021). Furthermore, particles > 125 µm account for a low proportion (cumulative volume) of the sample (≈10%, Figure S6). Previous analyses of TRWP have also shown that the average particle size is < 125 µm (Kreider et al., 2010; Klöckner et al., 2021 and Lundberg et al., 2020). The mesh sizes (125 and 20 µm) are commonly used for sieving analyses, and the use of those mesh sizes might enable a comparison with previous studies. Moreover, it is harder to obtain a statistically relevant result with the automated SEM/EDX single-particle analysis due to the relatively

low number of particles > 125 µm that can be analyzed in an analytical run considering the magnification used with a scanning electron microscope. The material collected in the 20-µm sieve (hereafter denoted 20−125 µm) was transferred onto Whatman Cyclopore Membrane filters (pore size 0.4 µm) by rinsing the sieve with de-ionized water (the sieve walls and the mesh was thoroughly rinsed to reduce the risk of loss of particles). The sieved liquid < 20 µm was filtrated on a separate Whatman filter. It means that the collected size fraction from the filtrate liquid < 20 µm comprises particles between 0.4 and 20 µm. However, out of this size fraction particles between 2 and 20 µm were analyzed (see Sect. 2.3.2). Therefore, this size range is hereafter denoted as 2−20 µm. The reason why particles smaller than 2 µm were not included in the analysis is because of the slow sedimentation rate of particles < 2 µm, which is therefore reflected in the sample preparation through dispersion (see Sect. 2.2.3), resulting in a sample that is underrepresented for particles < 2 µm. In addition, the smaller the particles, the less clear their morpho-textural fingerprint will be under the applied analytical conditions which are the best compromise for the entire analyzed particle size spectrum. With a decreasing particle size, the number of pixels per particle decreases, and the interaction volume of electrons and X-rays within the substrate—assuming a constant voltage—increases. All road dust samples were prepared in duplicates. For quality assurance and to estimate the contribution of particles suspended in the tap water or contaminants in the filters and the lab equipment, four blank samples containing one liter of tap water were filtered through Whatman Cyclopore Membrane filters (pore size 0.4 µm). Prior to the SEM analysis of the blank samples, the filters were coated with carbon, and single-particle analysis was performed on the filter surfaces.

#### *2.2.3 Dispersion of Particles on Boron Substrates*

Particles (i.e., < 20 µm, resp. 20–125 µm) were dispersed with compressed air using the Morphology G3ID device manufactured by Malvern. The dispersion was performed on a boron substrate (Rausch et al., 2022), which has the advantage of allowing the characterization and quantification of carbonaceous particles such as tire wear, bitumen, road markings, and biogenic/organics. This is possible because boron substrates do not contain the element carbon as ordinary substrates for SEM analysis.

### 2.3 SEM/EDX Manual and Automated Single-Particle Analysis

#### *2.3.1 Fingerprinting of Traffic-Derived Particle Subclasses Using Reference Materials*

To characterize the different particle types (especially new subclasses like bitumen, road markings, and glass beads) and obtain their characteristic morpho-textural-chemical fingerprint, reference material was analyzed manually and when possible, also in an automated manner. The reference material included road surface, road markings, and reflecting glass bead samples from different locations. Manual SEM/EDX analyses were performed on original pieces of reference material (Fig. 2a, b) that underwent no sample preparation (i.e., no milling, sieving, filtering, drying, or dispersion) apart from C-coating to guarantee sample conductivity during the SEM/EDX analysis. These untreated reference samples were analyzed to investigate the original composition, texture, distribution, and proportion of the different components within the reference material. Additionally, automated SEM/EDX analyses were performed on the same reference samples, that were—for this purpose—previously milled and dispersed on boron substrates as described in Sect. 2.2.3. The later sample preparation had the purpose of simulating samples with similar content as in road dust and collected in WDS road dust samples (i.e., comparable size range). By integrating the results of the reference samples in the particle classifier described in Sect. 2.4, the recognition of the newly characterized particles (bitumen, road markings, and glass beads) in the environmental WDS samples was facilitated.

#### *2.3.2 Automated SEM/EDX Single-Particle Analysis*

On average, 1137 particles per sample of the 20–125-µm fraction and 1324 particles per sample of the 2–20-µm fraction were analyzed by automated SEM/EDX single-particle analysis. For this purpose, a Zeiss Gemini 300 Field Emission Gun (FEG)-SEM equipped with an Oxford X-MAX EDS detector with an 80-$mm^2$ window, a high efficiency 4 quadrant backscatter electron (BSE) detector and the

**Table 1** Definition of the main- and subclasses differentiated by the ML-algorithm including their likely sources

| Main class | Subclass | Definition | Possible sources |
|---|---|---|---|
| Metallic particles | Metallic particles | Particles that mainly contain metals (very often Fe, Cu, Cr, Sb, Sn, Ba, and Si, O, etc.) | E.g., road/railway traffic (brake wear, railway wear), industry (recycling) |
| Road marking (paint) wear particles (Ti-bearing) | Road marking (paint) wear particles (Ti-bearing) | Particles consisting of a carbonaceous matrix rich in $TiO_2$ particles (sub-micron to nano-sized) | E.g., road traffic, other paints |
| Reflecting glass bead fragments | Reflecting glass bead fragments | Glass particles with a relatively homogeneous elemental composition (Si, O, Ca, Na, Mg, Ti, C) and angular morphologies (i.e., glassy shards) typical of fragments (i.e., wear) derived from reflecting glass beads or other glass products. C and Ti are stemming from the road marking matrix that can be attached to glass bead fragments | E.g., road traffic, other glass shards |
| Organic undifferentiated particles | Organic undifferentiated (i.e., biogenic/organic particles) | Particles that mainly contain carbon and oxygen with small amounts of ± nitrogen, sulfur, potassium, phosphor, calcium, sodium, etc | E.g., biogenic (spores, pollen), organic matter (plant fragments, undifferentiated organic matter) |
| Minerals | C-poor minerals | Particles showing a mineral fingerprint with little traces of supplementary carbon (often silicates, calcite, or mixtures). They can be single crystals or aggregates | e.g., road wear, construction work, quarries, geogenic |
| | C-rich minerals | Particles showing a mineral fingerprint with higher carbon concentrations than expected in pure minerals (silicates, calcite, or mixtures often mixed with or coated by bitumen and/or other organic material). They can be single crystals or aggregates | E.g., mixtures of minerals and bitumen derived from road wear mixtures of minerals with biogenic or undifferentiated organic matter |

**Table 1** (continued)

| Main class | Subclass | Definition | Possible sources |
|---|---|---|---|
| Carbon-dominated traffic-derived wear particles (tire and bitumen wear particles = TBiWP) | Tire wear particles (TWP) | Mixed particles consist of an organic-rich matrix (interpreted to be tire tread) and different proportions of minerals (for further information see 3.1.2 and 4). Particles can also contain metallic inclusions (e.g., from brake wear previously formed and deposited on the road surface) and/or bitumen wear. For further details on this particle subclass see (Rausch et al., 2022) | E.g., road traffic; particles originating from the abrasion process of tires upon contact with the road surface (which largely consists of minerals) |
| | Bitumen wear particles (BiWP) | Mixed particles consist of an organic-rich matrix (interpreted to be bitumen) and minerals (for further discussion see 3.1.3 and 4). Particles can also contain metallic inclusions (e.g., from brake wear previously formed and deposited on the road surface) and/or tread wear | E.g., road traffic; particles originating from the abrasion process of the road surface upon use |

particle analysis software AZtecFeature (©Oxford Instruments) was used at the Particle Vision lab (Fribourg, Switzerland). For each particle, a BSE image was taken and EDX analysis was performed. The analyses were performed at 12 kV, with a 60-µm aperture and approximately 3.4-nA beam current measured with a Farraday cup. The image pixel size for the analysis of the finer fraction (2–20 µm) was 0.056 µm (500 × magnification and resolution of 4096 × 3072 pixels per image). For the larger fraction (20–125 µm), 170 × magnification and a resolution of 4096 × 3072 pixels per image were used and the pixel size was 0.1644 µm. Particles on the boron substrate were recognized by gray value (i.e., BSE intensity) thresholding. EDX analyses were performed for each recognized particle with the AZtecFeature software (©Oxford Instruments). For further details on the SEM/EDX approach for automated single-particle analysis see Rausch et al. (2022). Together with the elemental composition, nine basic morphological parameters for each analyzed particle were automatically determined by the AZtecFeature software.

### 2.4 Data Treatment and Particle Classification with ML

The data sets obtained from the AZtecFeature software were exported and subsequently treated with a machine-learning (ML)-based algorithm (see supplementary material, Figure S1 and Figure S2). Besides the chemical and morphological (size, circularity, aspect ratio, etc.) parameters delivered by the AZtecFeature software, the algorithm originally developed for air samples automatically extracts and calculates 21 complementary morphological and textural (backscatter-signal based) parameters (e.g., fractal dimensions, convexity, gray kurtosis, modified Ripley's K-functions) (Rausch et al., 2022). For the particle classification, all the available chemical and morpho-textural descriptors (in total 67) are combined in a "random forest" model trained with 113,043 particles from 138 WDS samples and six air samples (Sigma-2 samples, from Stockholm, Sweden). Additionally, six reference samples created by mortaring material of different road paints were analyzed. The prediction accuracy that is expected from the developed ML-classifier and further details on the ML-model are shown in the Supplementary material (Figure S1). As a quality assurance of the

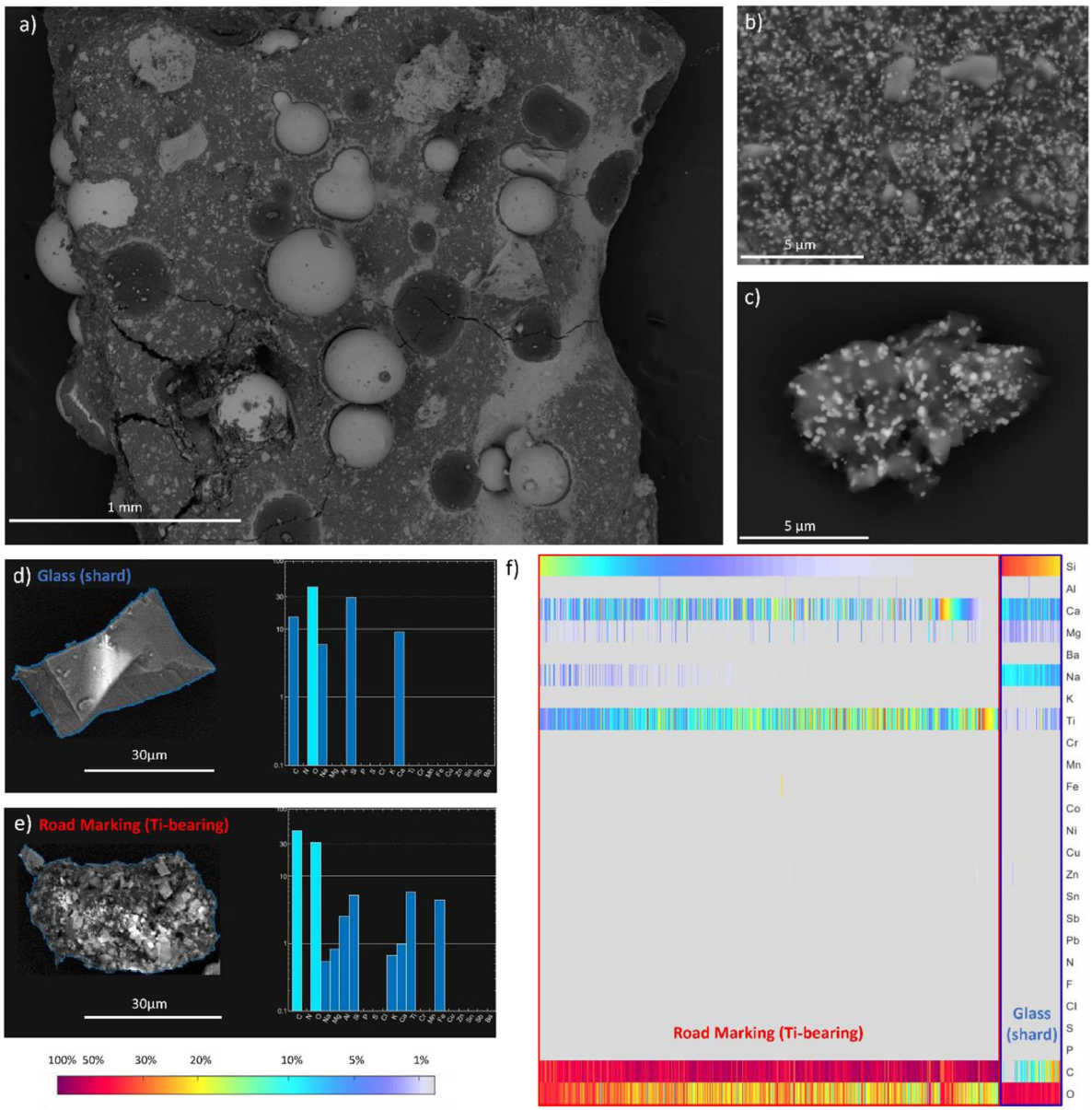


**Fig. 2** (**a**) Backscatter image of a piece of road marking containing glass bead and minerals. (**b**) Zoom-in of the dark matrix containing micrometric bright mineral particles and brighter Ti-bearing pigments submicron to nanoparticles. (**c**) Backscatter image of a single Ti-bearing road marking wear particle from the milled reference sample. (**d**)Backscatter image of a glassy shard with its corresponding typical elemental composition (histogram to the right). (**e**) Backscatter image of a road marking wear particle with its corresponding typical elemental composition (histogram to the right). (**f**) Heatmap obtained from the automated single-particle analysis of the milled road marking/glass bead reference sample showing the typical elemental composition of both, road markings and glass beads, and their proportion within the sample (see heatmap reading example in supplementary material, Figure S3)

particle classification, the image and elemental spectra of each particle can be manually double-checked. The classification of each particle is also labelled with a score that indicates the level of confidence of the classification within a certain class. Therefore, if desired, these tools can be used to manually evaluate the results and if necessary, perform changes by moving one particle to another particle class.

Subsequently, all quantitative results in tables and graphs can be automatically updated. Information on repeatability tests for quality assurance and detection limits can be found in supplementary material 1.1−1.4.

## 3 Results and Discussion

### 3.1 Fingerprinting of New Traffic-Derived Particle Subclasses

Under the backscatter detector, road marking (paint) wear consists of a matrix with embedded bright, nearly spherical particles (Fig. 2a) with a diameter of a few hundred microns (=glass beads). The matrices may also contain single minerals (see angular particles in micrometric size; Fig. 2a). On a submicro- to nanometric scale Ti-dominated particles are ubiquitous, which can be seen in more detail in Fig. 2b, c. The backscatter image shown in Fig. 2c shows a single Ti-bearing road marking wear particle stemming from the milled reference sample. This image reveals that Ti is homogenously distributed even in particles with a few micrometers. In the analyzed size ranges, glass particles are not represented by complete glass beads, but rather glassy shards (=fragments of a glass bead) with their corresponding typical elemental composition (Si, O, Ca, Na, C; Fig. 2d). Figure 2e shows another larger Ti-bearing road marking wear particle and its elemental composition typically dominated by C and O with lower and variable amounts of Ti, Fe, Si, Al, Mg, Ca, Na, and K. Finally, Fig. 2f is a visualization (heatmap) of the overall elemental composition, obtained from the automated single-particle analysis of the road marking/reflecting glass bead reference sample that was milled and prepared as described in Sect. 2.2.2. The heatmap (Fig. 2f) shows the typical elemental composition of both, road markings and glass bead fragments (see heatmap reading example in supplementary material, Figure S3). In addition, the approximate relative proportion of the two particle types within the original sample can also be extracted from this analysis (ca. 85% road marking wear particles vs. ca. 15% glass bead fragments, based on number concentrations).

The morpho-textural-chemical characteristics of bitumen wear particles determined in similar manner as for the above-described road marking and glass bead wear particles are discussed in detail in Sect. 3.2.5. These newly defined morpho-textural-chemical fingerprints were subsequently integrated into the classification schema of the machine-learning algorithm applied in this study. This made an automated identification and quantification of bitumen, road marking, and glass bead particles, besides the previously in Rausch et al., (2022) defined subclasses: minerals, metals, tire wear, and biogenic/organic, in road dust samples possible (see Sect. 3.2).

### 3.2 Automated Identification of Traffic-Derived Wear Particles

The road dust samples were classified into the following morpho-textural-chemical particle main classes: (a) organic undifferentiated particles, (b) minerals, (c) carbon-dominated traffic-derived wear particles (i.e., tire and bitumen wear particles TBiWP), (d) metallic particles, (e) paint/road marking wear, and (f) reflecting glass beads (Table 1, Fig. 2, Fig. 3). This differentiation was possible because even though all these environmental particles are characterized by a certain heterogeneity, each of the particle classes exhibits a specific and distinctive fingerprint if all the morpho-textural characteristics and information on elemental composition are combined. This is illustrated in Fig. 4, where a dimensionality reduction is aplied to the feature vectors of chemical, textural, and morphological properties of the 11,043 particles of the dataset: particles of the same class, which are expected to share similar characteristics in the high-dimensional space, naturally form clusters in a plane. We use the t-SNE algorithm for this unsupervised nonlinear 2D projection, since it is well suited for visualizing high-dimensional data. Moreover, some classes clearly exhibit subclasses (multiple neighboring subclusters within the same class), which correspond to specific morphologies and/or elemental compositions.

For example, subclasses of the mineral main class are C-rich minerals and C-poor minerals (Table 1, Fig. 2). Note that the dimensionality reduction is a convenient way to explore the dataset and confirm the relevance of the defined classes, but it is not a classification per se. All following results presented in this study are based on a random forest classifier; details about this algorithm are given in the supplementary material and elsewhere (Rausch et al., 2022).The typical morpho-textural characteristics of each particle

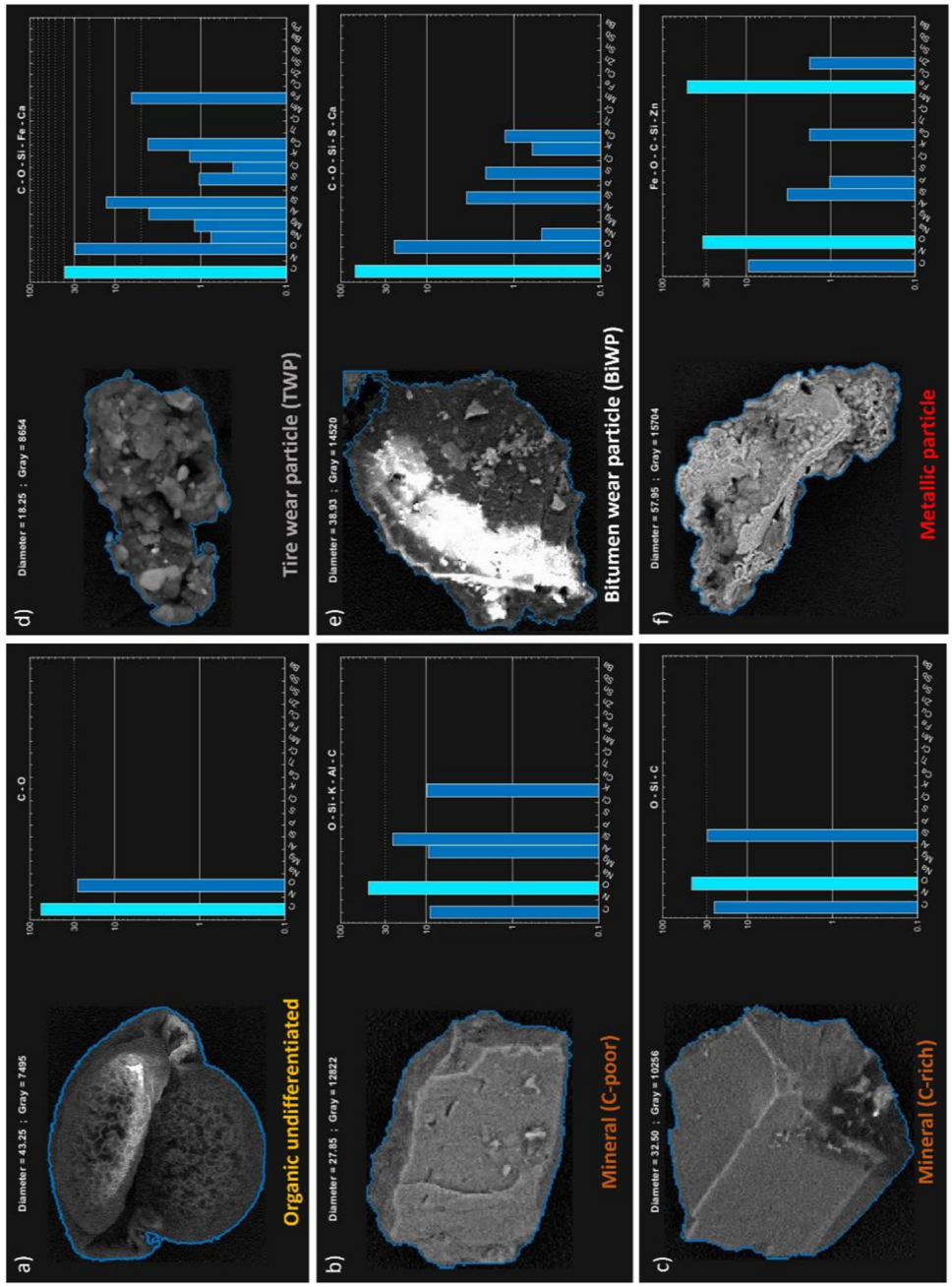


**Fig. 3** (**a–f**) Backscatter images of typical particles for the corresponding subclasses (see definition in Table 1). For the subclasses "road marking wear" and "glass bead fragments," the contextualization and their elemental composition are shown separately in Fig. 2


**Fig. 4** Unsupervised two-dimensional reduction (t-SNE algorithm) applied to the dataset (113,043 particles) of the road dust classification model. The multi-dimensional vectors of chemical, textural, and morphological properties of the particles are projected in a nonlinear way onto a 2D space: particles with similar characteristics in the high-dimensional space are located close to each other in the image. The main classes of the particles found in road samples are "naturally" clustered in this embedding. One can see that some classes, e.g., mineral particles, can be further separated into subclasses, which correspond to specific morphologies and/or chemical compositions, Figure S2

main-class/subclass are displayed exemplarily in the SEM images shown in Figs. 2 and 3, while the typical spectra of the elemental composition are summarized in the heatmap shown in Fig. 5.

In the following sections, the results and source interpretations obtained for each traffic-derived particle subclass will be discussed in detail considering the complete data set (i.e., both size fractions 20−125 µm and 2−20 µm together) as the two fractions show slight but not fundamental differences. These samples were collected at the road surface of Testsite E18.

#### *3.2.1 Metallic Particles (Brake and Vehicle Wear)*

The road dust samples (particularly the coarse fraction 20–125 µm) contain smaller proportions of metallic particles compared to mineral and TBiWP (Fig. 5). This is most likely related to the intrinsic particle size distribution of metallic particles in urban environments since they are highly concentrated in the fine fractions (median at about 2−4 µm) (Jayarathne et al., 2019; Pant & Harrison, 2013; Rausch et al., 2022). Since only particles > 2 µm were included in this study, it is likely that a noticeable fraction of metallic particles smaller than 2 µm are missing in these quantifications. The most dominant elements in the analyzed metallic particles are Fe followed by O, C, and Si. Additionally, metallic particles contain low concentrations of Al, Ca, Mg, Ti, Cr, Mn, Cu, Zn, and S. The obtained elemental compositions and size range are in good agreement with the expected composition and size of brake wear particles (Harrison et al., 2021; Vojtíšek-Lom et al., 2021). Brake discs are normally dominated by iron (Fe), while brake pads have a more variable composition. Dominating metals are Ba, Cu, Fe, Mn, Ti, and Zn (e.g., Grigoratos & Martini, 2014), while others are present in lower concentrations, like Sb, Cr, Ni, K, Si, Pb, Mo, and Sn (e.g., Figi et al., 2011; Sethupathi et al., 2021). Metals as Fe, Cu, Ba, and Sb are commonly used as markers for brake wear (Pant & Harrison, 2013). Even though metallic particles were not the focus of this study, their importance as an environmental pollutant, possibly with major health effects (Daellenbach et al., 2020), is worth mentioning. Their further investigation and monitoring are also of crucial importance in the light of expected upcoming regulations involving brake wear.

#### *3.2.2 Reflecting Glass Beads and Road Marking Wear*

The glass beads, tend to be larger (several hundred microns) than the largest analyzed particles (see Fig. 2a) and mainly glass shards were found in the road dust. The elemental composition of glassy wear particles stemming from reflecting glass beads is fairly homogeneous (Si, Ca, Na, O ± Mg) while road markings show a higher heterogeneity, which depends on the proportion of minerals (e.g., calcite and silicates) and $TiO_2$ pigment embedded in the carbonaceous matrix (Fig. 2d). A clear diagnostic criterion to identify road marking wear particles is the ubiquity of Ti ranging from a few % to up to about 36 wt.% in this case-study. Moreover, the element Ti is widely distributed in the C-rich matrix as sub-micron to nanoparticles (white pigments) (Fig. 2b, c, f). This is the reason why road marking wear particles are also readily detectable in the fine fraction. Kole et al. (2017) estimated that 5% of the total amount of road markings is released into the environment on an annual basis. The wear rate is higher in countries where salt, winter maintenance, and studded tires are in use. Little is known about the actual concentrations of road markings in different sample media, thus TWP and road marking polymers have seldom been analyzed in parallel. Horton et al. (2017) found road marking particles (red or yellow particles with glass beads incorporated) in sediment samples from the Thames River basin. However, the particles were larger (1–4 mm) than the particles analyzed in the present study. Vogelsang et al. (2019) found yellow particles (50–2000 µm) in road dust assumed to be road marking particles, and Zannoni et al. (2016) found road paint and glass beads in road dust collected adjacent to the kerb and in-between the wheeltracks. For this study, white particles and shards stemming from glass beads were commonly found in both fractions of the road dust samples. Furthermore, a large number of road marking particles were visually identified in the > 125 µm-fraction. However, this fraction was not further analyzed in this study.

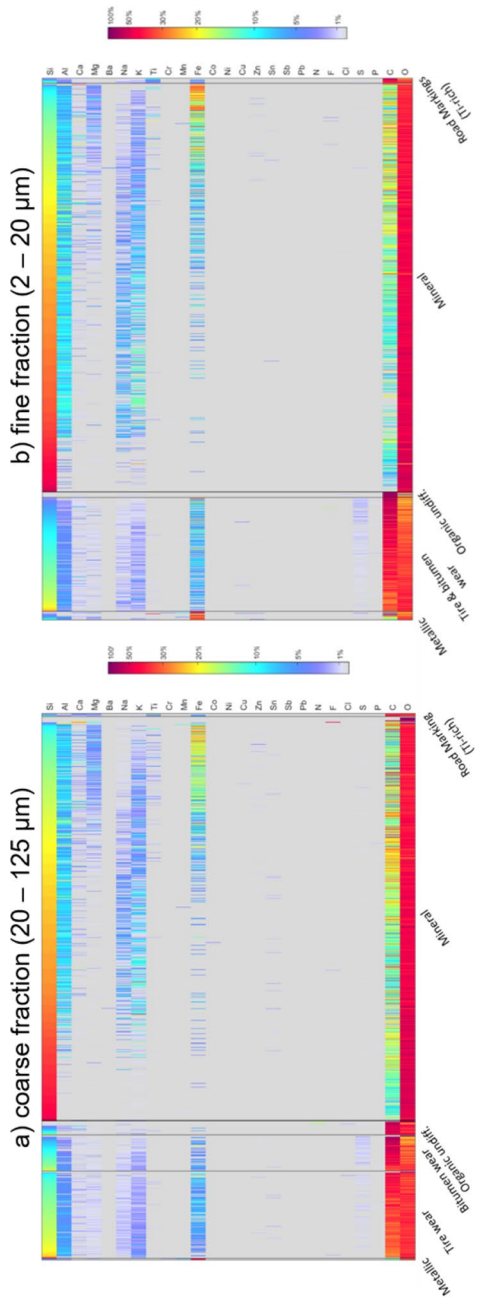


**Fig. 5** (**a**) Heatmap showing the elemental composition of 11,376 particles analyzed in the coarse fraction (20–125 µm) of ten road dust samples. Particles are organized after the main classes defined in Sect. 2.4., whereas the subclasses TWP and BiWP are additionally shown. (**b**) Heatmap showing the elemental composition of 13,244 particles analyzed in the fine fraction (2–20 µm) of the WDS samples. Particles are organized after the main classes defined in Sect. 2.4

### 3.2.3 Road Wear (Mineral Particles)

The results show that mineral particles are by far the most dominant components of road dust throughout the complete analyzed size spectrum (Fig. 5). Mineral particles collected from the road surface at Testsite E18 show a wide spectrum of elemental compositions. However, all mineral particles contain silica in variable proportions (i.e., silicates), and practically no carbonates were found. The bedrock in Sweden contains little carbonates in general; however, if samples from an area with more limestone had been analyzed (e.g., samples from the Alps or the Dolomites), the proportions of carbonates had increased. The majority of the mineral particles consist of Si, O, Al, K ±, Na, Fe, Mg, and Ti. Minerals containing only Si and O ± low concentrations of C (i.e., most likely quartz) are also present, even though in lower concentrations. The carbon content in quartz and other mineral particles is most likely mainly related to the coating of organic matter on the particle surface and partially due to an overestimation of the element carbon by the EDX measurement. The elemental combinations shown in Fig. 5 suggest that the mineral particles mainly consist of feldspars, amphibole, biotite, and quartz, minerals abundant in Swedish bedrock and used in the road wearing courses. The high silica content of the rocks used in the pavement mineralogy indicates that they are the main source of minerals found in the WDS samples. The soils surrounding the sampling site are farmland covered with crops, except during the winter months, with a high organic content and are therefore considered a weaker mineral source. Also, based on transect measurements presented in a companion study (Järlskog et al., submitted), most of the minerals measured in the context of this study seem to be originating from the road surface (i.e., road wear), since the absolute concentration of mineral particles decreases with increasing distance to the road. The abundance of road wear particles in the analyzed samples is not surprising if we consider that road wear is an important component in non-exhaust emissions (e.g., Casotti Rienda and Alves (2021) and Piscitello et al. (2021)) and can be especially dominant in areas where studded tires are used in winter, like in the Nordic countries (e.g., Kupiainen et al. (2016)). Morphologically, these particles are fragments in grainy, flaky, or shard-like shapes as previously described by Gustafsson et al. (2008). A small fraction of road wear is made up of the binder, approximately 4−8%, which in asphalt pavements is bitumen, with additives like resins, fibers, and stone flour (Asphalt Institute, 2014). Further details on bitumen particles are discussed below. Road wear particles are dominated by the coarser size mode (Figure S6) but range from about 0.2−2000 µm.

### 3.2.4 Tire Wear Particles

Tire wear particles from the road dust samples show basic common morpho-textural-chemical characteristics as described for airborne TWP in Rausch et al. (2022). Here, TWP were also dominated by C, O, and Si, which are typical elements of pristine tires. Besides these elements, they contain low concentrations of Fe, Al, K, Na, and sometimes Mg, Ca, and S. Interestingly, only very few particles contain Zn and less than in air samples (Rausch et al. (2022)). One possible explanation could be that Zn becomes leached into the aquatic phases as suggested by Degaffe and Turner (2011). Furthermore, the elements present in TWP (besides the ones stemming from the tread, i.e., C, O, and Si) coincide with the elements found in the mineral particles (see above). This is further evidence for the statement presented in several articles that environmental TWP occur as mixtures of tread and mineral encrustations (Halle et al., 2021; Kovochich et al., 2021; Kreider et al., 2010; Rausch et al., 2022; Sommer et al., 2018). In this case, the correlation between mineral encrustations and available minerals on the road is proved. Notably, the chemical fingerprint of airborne TWP in Switzerland (Rausch et al., 2022) differs in three aspects: (i) practically all TWP in the Swiss samples contain Ca, while this element is largely lacking in the E18 Swedish samples; (ii) the opposite behavior can be observed for K, which is much less common in the Swiss TWP; (iii) the relative C-content of the WDS Swedish TWP was found to be slightly lower. The first two divergences (i–ii) can be explained by the different types and compositions of available and used rock types in the roads at the different studied sites (most of the minerals found in the Swiss airborne samples also coincide with the road composition at the studied sites and with the elements present in the TWP). The last discrepancy (iii) is interpreted to be due to a larger enrichment of minerals on the particle surface of the WDS Swedish TWP (observed

during SEM analysis). It is hypothesized that this occurs because the particles sampled with the WDS were longer time on the road surface and could be repeatedly reworked, while the airborne TWP that reach the sampler had probably less interaction with the mineral dust on the road surface.

Additionally, it was observed that the morphology and texture of the TWP from the present study seem to be less pristine (e.g., reflected in a less cloud-like and fresh appearance) in comparison with the observations performed in previous studies for airborne samples (Rausch et al., 2022; Sommer et al., 2018) and in the Swedish Sigma-2 airborne samples presented elsewhere (Järlskog et al., submitted). This might be related to alteration, leaching, and possible aging processes occurring on the road surface, which is influenced by weathering processes induced by rain, snow, and solar radiation. Recently published studies have also observed that environmental TWP differ in chemical composition and morphology compared to pristine TWP (Halle et al., 2021; Kovochich et al., 2021; Sommer et al., 2018; Wagner et al., 2022). Several articles have described environmental TWP as elongated particles with mineral encrustations (Adachi & Tainosho, 2004; Kreider et al., 2010; Williams & Cadle, 1978). However, Kovochich et al. (2021) presented both elongated and near-spherical TWP. This was also confirmed by Rausch et al., (2022), where the authors present TWP with different morphologies (i.e., both elongated and spherical). In Fig. 6, the confrontation between aspect ratio and equivalent circular diameter (ECD) is presented for all identified TWP in both size fractions. No obvious correlation was detected, indicating that elongation is not related to particle size.

### *3.2.5 Bitumen Wear Particles*

The difference in the elemental composition between TWP and BiWP is very subtle. This is one of the reasons why the differentiation of these particle subclasses is very challenging. The main elemental differences between both particle types are that BiWP tend to have slightly higher C- and S-concentrations than TWP (Fig. 5). The other main elements in BiWP (Si, Fe, Al, K, ± Na, Mg, Ca, and S) coincide not only with the major elements in the TWP but also in the mineral particles, which is supplementary evidence for the road wear origin of most of the mineral

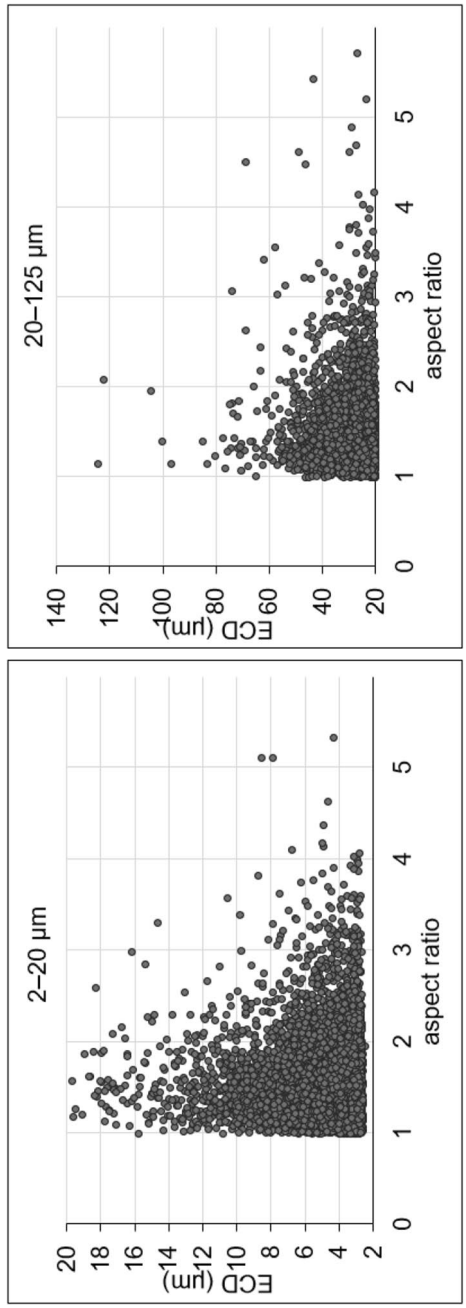


**Fig. 6** TWP morphology. Aspect ratio vs. particle diameter (ECD, equivalent circular diameter) for all analyzed TWP in the fine (2–20 µm) and coarse (20–125 µm) fractions

particles measured in these samples, as BiWP are clearly derived from the road surface containing this mineral-bitumen mixture. Diagnostic criteria helping to differentiate BiWP and TWP (especially in the coarser fraction) are the morpho-textural characteristics. BiWP have a darker matrix on BSE-images (reflecting high C-content and hence low-density material). In addition, large mineral encrustations are very common in the particles of the coarse fraction resulting in more angular morphologies of the BiWP and particles showing large contrasts between dark and bright materials, which often manifest under the SEM with charging effects (see Fig. 2e and Fig. 8). Even though this effect is not desirable when aiming for high-qualitative images, it can be used as an advantage for BiWP differentiation. BiWP is the only subclass that could not be satisfactorily differentiated in the small fraction (2−20 µm).

### 3.2.6 *Challenges in the Differentiation of Tire Wear Particles and Bitumen Wear Particles*

In the case of the main class "carbon-dominated traffic-derived wear particles", there is a supplementary complexity since it contains the two subclasses "tire wear" and "bitumen wear", therefore called TBiWP, which are chemically and morpho-texturally very close to each other. The endmembers of these two subclasses present clear differences in terms of morphology, texture, and elemental composition (Fig. 2d, e, Fig. 5, and Fig. 7). However, it is also evident that between the endmembers, a

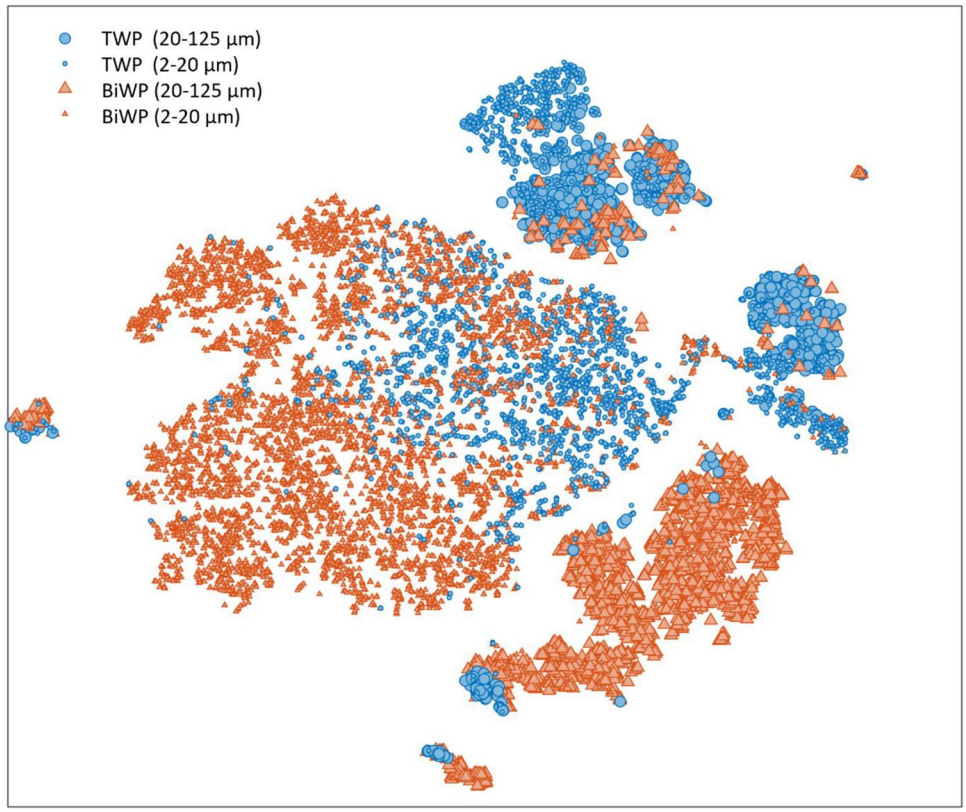


**Fig. 7** The unsupervised two-dimensional reduction (t-SNE algorithm) applied to the TWP and BiWP particles. This dataset is extracted from the main dataset of all particles by applying the road dust classification model. The multi-dimensional vectors of chemical, textural, and morphological properties of the particles are projected in a nonlinear way onto a 2D space: particles with similar characteristics in the high-dimensional space are located close to each other in the image. This graph shows that large particles (20–125 µm) tend to build better defined clusters than small particles (2–20 µm) before the classification model is applied. This illustration visualizes the larger difficulties in differentiating between TWP and BiWP in the small fraction and is the reason why the small fraction was not further subdivided

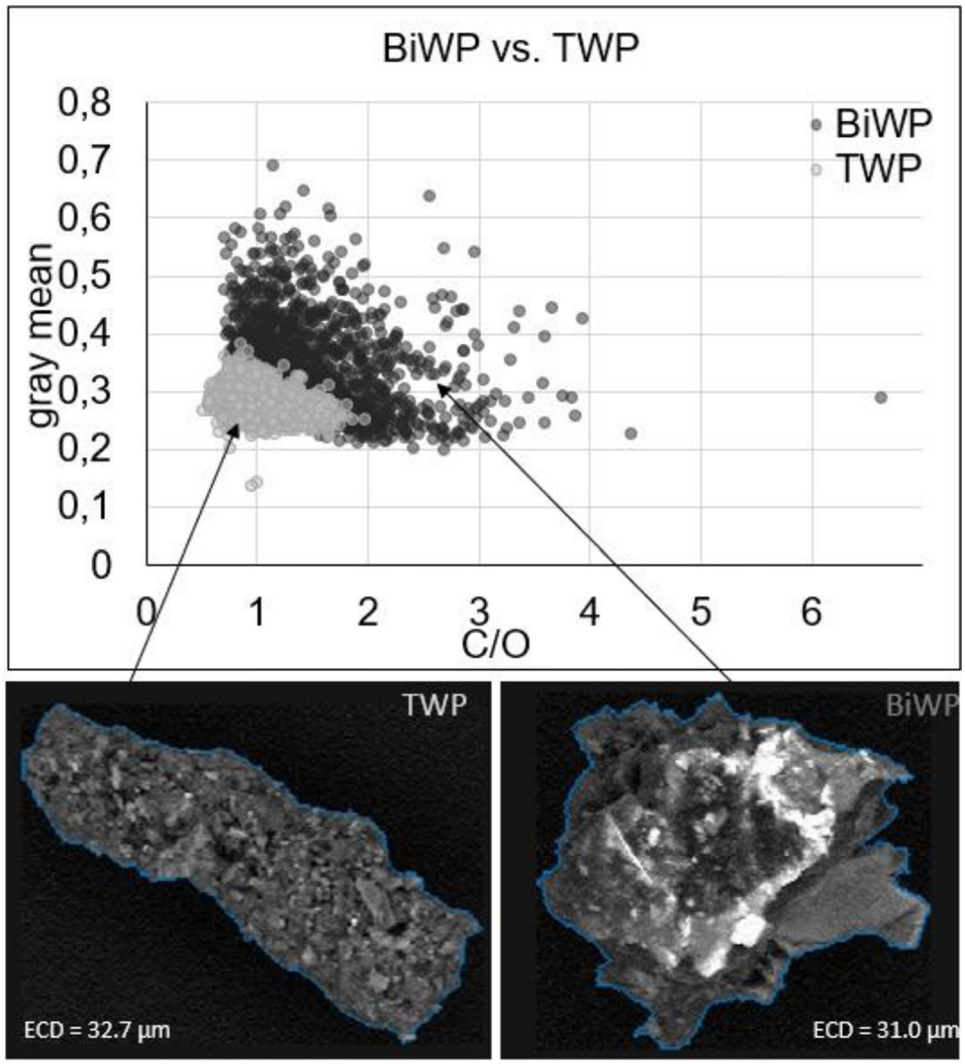


**Fig. 8** Graph showing the endmembers and mixing region (i.e., broad cluster) of TWP and BiWP after classification of the 20−125-µm particles. *X*-axis: carbon/oxygen ratio; *y*-axis: gray mean value for each particle (the value 0 represents the black color and value 1 represents the white color). In total, data for 3691 TWP and 1559 BiWP are shown. ECD, equivalent circular diameter in microns

complex mixing of environmental TWP and BiWP occurs visible as a continuum cluster in Fig. 7. Consequently, the differentiation of these mixtures is challenging and subjected to higher uncertainty. With the ML-algorithm, the particles will be classified in the subclass that based on the training set appears to be dominating and/or most likely even though they could be mixtures. Additionally, the smaller the particles, the less clear the textural fingerprint of these two subclasses (see large cluster consisting of both small (2−20 µm) TWP and BiWP in the center of Fig. 7), since they for instance contain less large mineral incrustations vs. groundmass. And due to the applied analytical conditions (which are the best compromise for the entire analyzed particle size spectrum), the specific characteristics of the groundmass become less visible with decreasing particle size (larger interaction volume of electrons and X-rays in smaller particles with a given voltage). The abovementioned observations are evidenced in Fig. 7, which shows the projection of the multi-dimensional vectors

of chemical, textural, and morphological properties of all analyzed TWP and BiWP in a nonlinear way onto a 2D space. Note that particles with similar morpho-textural-chemical characteristics are located close to each other in this image. So, that the mixed region mainly consisting of small particles clearly shows the greater difficulty, and therefore, uncertainty in differentiating TWP and BiWP, in the finer fraction. Therefore, the quantification of the subclasses TWP and BiWP needs to be seen as an approximate estimate, while the values obtained for the main class TBiWP represent robust results since this particle main class can be clearly differentiated from the other traffic-derived main classes (i.e., minerals, road markings, reflecting glass beads, and metallic particles), as well as from naturally occurring C-rich particles (i.e., biogenic/organic material) (see Figure S1) (Fig. 8).

### 3.3 Particle Size Distribution and Relative Proportion of the Different Particle Subclasses

The particle size distributions (frequency distribution) of the road dust samples show a peak at about 20–30 µm (Fig. 9). Only a small fraction of the particles is coarser than 200 µm, and the cumulative distribution (Figure S6) confirms that the majority of the particles are also finer than 125 µm (approximately 90%), indicating that the analytical focus should be on the finer fractions. An additional motivation to focus on this size fraction is that it has often been excluded in previous work due to analytical difficulties. Therefore, it was prioritized to develop a method that was able to differentiate between different subclasses also in the < 125-µm fraction.

Similar results were found in Kovochich et al. (2021) where TRWP generated from a road simulator

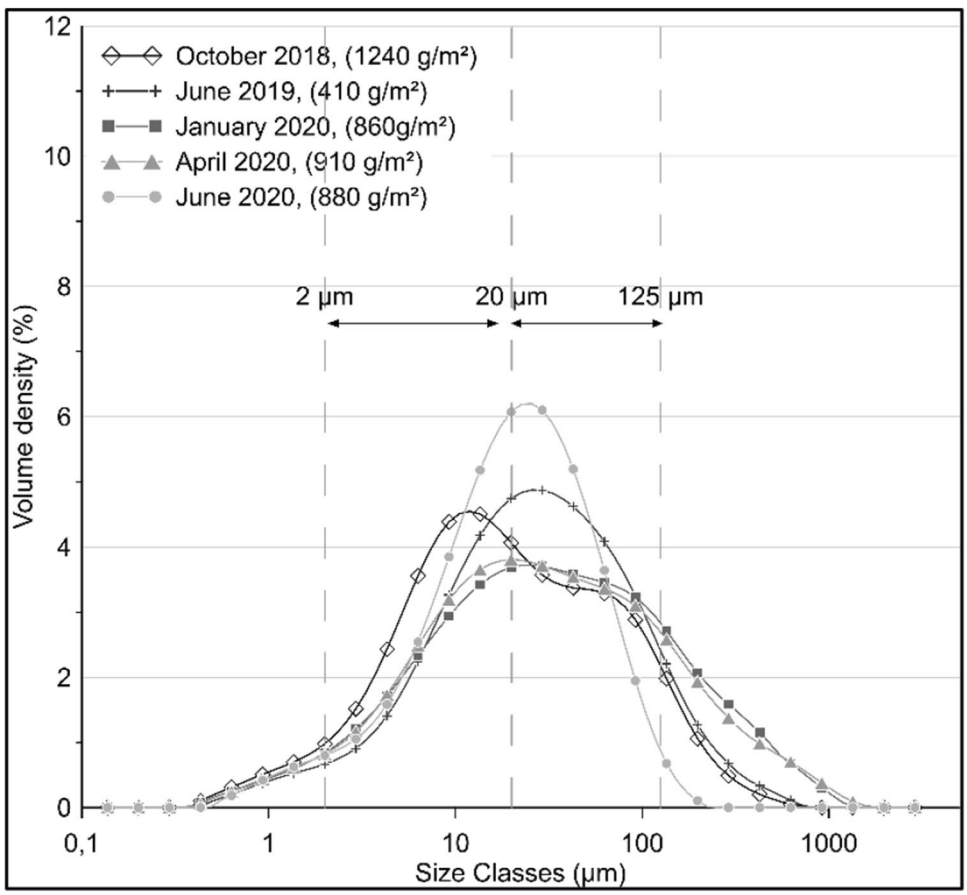


**Fig. 9** Particle size distribution for the road dust samples. The values within the brackets are the amount of road dust (g/m.$^2$)

were analyzed. Their results showed that in average TRWP have a diameter of 49 µm (34 µm by number distribution). The PSD was similar to those found in Kreider et al. (2010) (75–100 µm), Klöckner et al. (2021) (20–50 µm), Lundberg et al. (2020) (10–80 µm), and Järlskog et al. (2020) (50 µm). The total mass of particles < 2000 µm (g/m$^2$) in the road dust samples of this study varied between 400 and 1240 g/m$^2$ ($\bar{x}$ 860 g/m$^2$) (Fig. 9), which is within the same mass range as Rødland et al. (2022b) found in urban roadside snow. The high particle loads are related to the long-term accumulation of road dust at the curb, where the samples were taken. These results support our decision to not include particles > 125 µm in the present study especially since coarser particles tend to deposit close to the source while finer particles are further transported into the environment. However, 10% of the road dust were still coarser than 125 µm, resulting in potential underestimations if the total emissions are calculated only based on the present results.

A total of ten road dust samples were analyzed. The results showed a relative number concentration of the particle classes similar in the coarse and the fine fractions, with minerals as the most dominant particle class (2–20 µm $\bar{x}$ = 78%, 20–125 µm $\bar{x}$ = 74%) followed by the sum of Trip (2–20 µm $\bar{x}$ = 19%, 20–125 µm $\bar{x}$ = 22%). The relative composition of metallic particles was higher in the fine fraction (2–20 µm $\bar{x}$ = 1.3%, 20–125 µm $\bar{x}$ = 0.4%), and the organic material was slightly higher in the coarse fraction (2–20 µm $\bar{x}$ = 0.8%, 20–125 µm $\bar{x}$ = 2.5%). Road marking wear particles made 1% in the fine fraction and 0.5% in the coarse fraction, while glass beads wear contributed 0.1% and 0.2% in the fine and coarse fractions, respectively (Fig. 10).

In the coarse fraction, where TWP and Bow were differentiated, it was observed that TWP ($\bar{x}$ = 15%) had in average a slightly higher contribution to the analyzed road dust samples than Baw ($\bar{x}$ = 7%). Even though TWP and bow were not quantified separately in the fine fraction, similar trends are well visible also in this fraction, i.e., the relative concentrations of TBiWP were in the same range as the relative concentrations of BiWP and TWP (together) in the coarser fractions (10) (Relative mass concentrations and total number of particles can be seen in Table S2).

Previously published studies on TWP in road dust samples have mainly used thermal methods for quantification (e.g., Kreider et al., 2010; Kumata et al., 2000, 2011; Parker-Jurd et al., 2021; Rogge et al., 2012; Unice et al., 2013; Youn et al., 2021), which make it difficult to compare the results with the present study due to different size ranges, set-ups, sample preparations, and units used.

Nevertheless, as a quality check, the following comparison between methods was performed. Environmental samples that were collected for Järlskog et al. (2021), and previously analyzed with light microscopy were analyzed in the present study with SEM/EDX, see Supplementary material, Table S3. The comparison indicated that the methods gave similar results in the very coarse fraction (100−300 µm). In the coarse fraction (20−100 µm), the light microscopy tended to underestimate the number of particles compared to the SEM/EDX, (Table S3, as also indicated and discussed in (Järlskog et al., 2021)). The main limitations of manual particle counting in the fine fractions can be attributed to (i) the large number of particles that need to be counted, (ii) the lower size resolution of the light microscopy method, and (iii) the eyesight and concentration of the operator, which can be further influenced the longer the analysis takes. However, light microscopy can still be a suitable and reliable method for coarser particles and to give a first indication of the composition of a sample.

## 4 Conclusions

To our knowledge, this is the first study that differentiates between TWP, BiWP, and road markings (all being carbon-rich traffic-derived wear particles) besides other traffic-derived particles containing low carbon concentrations, such as brake wear, mineral road wear, and reflecting glass beads in environmental (i.e., real-world) road dust samples. The SEM/EDX/ML method showed high repeatability and an accurate classification into the different subclasses. It also showed promising results for future application studies addressing specific research questions (e.g., transport and spread of traffic-derived particles including MP in the various environmental compartments) and can be used as a rapid and repeatable technique for environmental samples and monitoring studies.

One interesting observation is that the relative number concentrations of the particle classes within the coarse and the fine fractions are very similar. Minerals, interpreted to be largely derived from

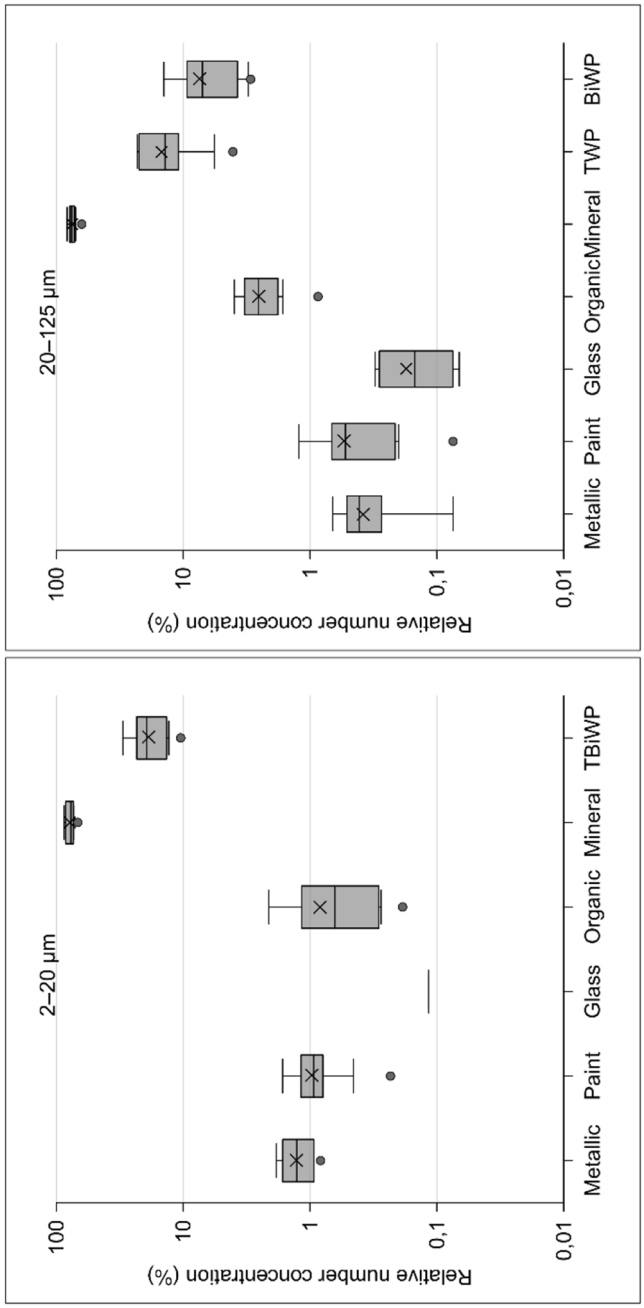


**Fig. 10** Relative number concentration (%) of the different particle subclasses quantified in the road dust samples shown as boxplots (number of samples = 10 NB glass was only detected in 1 out of 10 samples in the fine fraction). The results of the fine fraction, 2–20 µm, are presented to the left and of the coarse fraction, 20–125 µm, to the right. The edges of the boxes represent the 25 and 75 quartiles; the whiskers represent the 10 and 90 percentiles. The cross within the boxes shows the mean value, and the line shows the median. The small dots are the outliers

road abrasion, are the most dominant particle class (> 70%) followed by TBiWP (ca. 20%), in both fractions. Road marking wear made in both size fractions < 1%, while glass bead wear particles showed the lowest concentration (< 0.1%) of all differentiated classes. The relative contribution of metallic particles was slightly higher in the fine fraction with average values ranging between 0.3 and 1.3%, and the organic material was slightly higher in the coarse fraction contributing with average values between 0.8 resp. 2.5%. The results presented in this study show that a considerable amount of the road dust analyzed (both the coarse and the fine fraction) consists of TWP and BiWP and confirm that they are important sources of wear particles and MP pollution in the environment. Even though in smaller concentrations, road marking and glass bead wear also contribute to road dust in the complete analyzed size range.

The particle size distribution of the road dust samples indicates that the majority of the traffic-derived non-exhaust particles are < 50 µm, highlighting the importance to analyze particles in the fine fraction in environmental samples. This automated SEM/EDX ML-based technique can be used as a complement to other analytical techniques able to differentiate polymer species (e.g., FTIR, pyr-GC/MS, TED-GC/MS), when there is an interest to get a deeper understanding of the particle size, morphology, particle encrustations, and overall composition of the sample.

**Funding** Open access funding provided by Swedish National Road and Transport Research Institute (VTI). This work was supported by the Swedish Research Council for Environment, Agricultural Sciences and Spatial Planning (Formas) (Reg.No. 2017–00720) and the Swedish Government (N2017/07856/SUBT).

**Data Availability** The datasets generated during and/or analyzed during the current study are available from the corresponding author on reasonable request.

**Declarations**

**Conflict of Interest** The authors declare no competing interests.



## References

Abbasi, S., Keshavarzi, B., Moore, F., Delshab, H., Soltani, N., & Sorooshian, A. (2017). Investigation of microrubbers, microplastics and heavy metals in street dust: A study in Bushehr city, Iran. *Environmental Earth Sciences*, *76*. https://doi.org/10.1007/s12665-017-7137-0

Adachi, K., & Tainosho, Y. (2004). Characterization of heavy metal particles embedded in tire dust. *Environment International, 30*, 1009–1017. https://doi.org/10.1016/j.envint.2004.04.004

Asphalt Institute. 2014. MS-2 Asphalt mix design methods. Vol 7th Edition: Asphalt Institute, 2014

Baensch-Baltruschat, B., Kocher, B., Stock, F., & Reifferscheid, G. (2020). Tyre and road wear particles (TRWP) - A review of generation, properties, emissions, human health risk, ecotoxicity, and fate in the environment. *Science of the Total Environment, 733*, 137823. https://doi.org/10.1016/j.scitotenv.2020.137823

Beddows, D. C. S., & Harrison, R. M. (2021). PM10 and PM2.5 emission factors for non-exhaust particles from road vehicles: Dependence upon vehicle mass and implications for battery electric vehicles. *Atmospheric Environment*, *244*. https://doi.org/10.1016/j.atmosenv.2020.117886

Bondelind, M., Nguyen, A., Sokolova, E., Björklund, K. (2019). Transport of traffic-related microplastic particles in receiving water. In: *Mannina G*. Springer International Publishing, pp. 317–321

Casotti Rienda, I., & Alves, C. A. (2021). Road dust resuspension: A review. *Atmospheric Research*, *261*. https://doi.org/10.1016/j.atmosres.2021.105740

Daellenbach, K. R., Uzu, G., Jiang, J., Cassagnes, L. E., Leni, Z., Vlachou, A., Stefenelli, G., Canonaco, F., Weber, S., Segers, A., Kuenen, J. J. P., Schaap, M., Favez, O., Albinet, A., Aksoyoglu, S., Dommen, J., Baltensperger, U., Geiser, M., El Haddad, I., … Prévôt, A. S. H. (2020). Sources of particulate-matter air pollution and its oxidative potential in Europe. *Nature, 587*, 414–419. https://doi.org/10.1038/s41586-020-2902-8

Degaffe, F. S., & Turner, A. (2011). Leaching of zinc from tire wear particles under simulated estuarine conditions. *Chemosphere, 85*, 738–743. https://doi.org/10.1016/j.chemosphere.2011.06.047

Eisentraut, P., Dümichen, E., Ruhl, A. S., Jekel, M., Albrecht, M., Gehde, M., & Braun, U. (2018). Two birds with one stone—Fast and simultaneous analysis of microplastics: Microparticles derived from thermoplastics and tire wear. *Environmental Science & Technology Letters, 5*, 608–613. https://doi.org/10.1021/acs.estlett.8b00446

Folkeson, L. (2005). Dispersal and effects of heavy metals from roads and road traffic: Literature survey. VTI Report, 512. Swedish National Road and Transport Research Institute (VTI).

Fugili, R., Nagel, O., Tuchschmid, M., Lienemann, P., Gfeller, U., & Bukowiecki, N. (2011). A tough nut to crack: Quantitative analysis of heavy metals in automotive brake linings. *Chimia, 65*, 275. https://doi.org/10.2533/chimia.2011.275

Goßmann, I., Halbach, M., & Scholz-Böttcher, B. M. (2021). Car and truck tire wear particles in complex environmental samples – A quantitative comparison with "traditional" microplastic polymer mass loads. *Science of the Total Environment, 773*, 145667. https://doi.org/10.1016/j.scitotenv.2021.145667

Grigoratos, T., & Martini, G. (2014). Brake wear particle emissions: A review. *Environmental Science and Pollution Research*. https://doi.org/10.1007/s11356-014-3696-8

Gustafsson, M., Blomqvist, G., Gudmundsson, A., Dahl, A., Swietlicki, E., Bohgard, M., Lindbom, J., & Ljungman, A. (2008). Properties and toxicological effects of particles from the interaction between tyres, road pavement and winter traction material. *Science of the Total Environment, 393*, 226–240. https://doi.org/10.1016/j.scitotenv.2007.12.030

Gustafsson, M., Blomqvist, G., Järlskog, I., Lundberg, J., Janhäll, S., Elmgren, M., Johansson, C., Norman, M., & Silvergren, S. (2019). Road dust load dynamics and influencing factors for six winter seasons in Stockholm, Sweden. *Atmospheric Environment: X*, *210*. https://doi.org/10.1016/j.aeaoa.2019.100014

Halle, L. L., Palmqvist, A., Kampmann, K., Jensen, A., Hansen, T., & Khan, F. R. (2021). Tire wear particle and leachate exposures from a pristine and road-worn tire to Hyalella azteca: Comparison of chemical content and biological effects. *Aquatic Toxicology, 232*, 105769. https://doi.org/10.1016/j.aquatox.2021.105769

Harrison, R. M., Allan, J., Carruthers, D., Heal, M. R., Lewis, A. C., Marner, B., Murrells, T., & Williams, A. (2021). Non-exhaust vehicle emissions of particulate matter and VOC from road traffic: A review. *Atmospheric Environment, 262*, 118592. https://doi.org/10.1016/j.atmosenv.2021.118592

Hjortenkrans, D. S. T., Bergbäck, B. G., & Häggerud, A. V. (2007). Metal emissions from brake linings and tires: Case studies of Stockholm, Sweden 1995/1998 and 2005. *Environmental Science & Technology, 41*, 5224–5230. https://doi.org/10.1021/es070198o

Holý, M., & Remišová, E. (2019). Analysis of influence of bitumen composition on the properties represented by empirical and viscosity test. *Transportation Research Procedia, 40*, 34–41. https://doi.org/10.1016/j.trpro.2019.07.007

Horton, A. A., Svendsen, C., Williams, R. J., Spurgeon, D. J., & Lahive, E. (2017). Large microplastic particles in sediments of tributaries of the River Thames, UK – Abundance, sources and methods for effective quantification. *Marine Pollution Bulletin, 114*, 218–226. https://doi.org/10.1016/j.marpolbul.2016.09.004

ISO. (2017a). *ISO/TS 20593: Ambient air — Determination of the mass concentration of tire and road wear particles (TRWP) - Pyrolysis-GC-MS method*. International Organization for Standardization.

ISO. (2017b). *ISO/TS 21396: Rubber — Determination of mass concentration of tire and road wear particles (TRWP) in soil and sediments — Pyrolysis-GC/MS method*. International Organization for Standardization.

Järlskog, I., Strömvall, A. M., Magnusson, K., Gustafsson, M., Polukarova, M., Galfi, H., Aronsson, M., & Andersson-Sköld, Y. (2020). Occurrence of tire and bitumen wear microplastics on urban streets and in sweepsand and washwater. *Science of the Total Environment*, *729*. https://doi.org/10.1016/j.scitotenv.2020.138950

Järlskog, I., Strömvall, A.-M., Magnusson, K., Galfi, H., Björklund, K., Polukarova, M., Garção, R., Markiewicz, A., Aronsson, M., Gustafsson, M., Norin, M., Blom, L., & Andersson-Sköld, Y. (2021). Traffic-related microplastic particles, metals, and organic pollutants in an urban area under reconstruction. *Science of the Total Environment, 774*, 145503. https://doi.org/10.1016/j.scitotenv.2021.145503

Jayarathne, A., Egodawatta, P., Ayoko, G. A., & Goonetilleke, A. (2019). Transformation processes of metals associated with urban road dust: A critical review. *Critical Reviews in Environmental Science and Technology, 49*, 1675–1699. https://doi.org/10.1080/10643389.2019.1579630

Jekel, M. (2019). Scientific report on tyre and road wear particles, TRWP, in the aquatic environment. European TRWP Platform, ETRMA, 2019. https://www.tyreandroadwear.com/wp-content/uploads/2019/10/FINAL-Scientific-Report-on-Tyre-and-Road-Wear-Particles.pdf

Jonsson, P., Blomqvist, G., & Gustafsson, M. (2008). Wet dust sampler: Technological innovation for sampling particles and salt on road surface. Seventh International Symposium on Snow Removal and Ice Control Technology, Transportation Research Circular; E-C126: 102–111.

Klöckner, P., Seiwert, B., Weyrauch, S., Escher, B. I., Reemtsma, T., & Wagner, S. (2021). Comprehensive characterization of tire and road wear particles in highway tunnel road dust by use of size and density fractionation. *Chemosphere, 279*, 130530. https://doi.org/10.1016/j.chemosphere.2021.130530

Kole, J. P., Löhr, A. J., Van Belleghem, F. G. A. J., & Ragas, A. M. J. (2017). Wear and tear of tyres: A stealthy source of microplastics in the environment. *International Journal of Environmental Research and Public Health*, *14*. https://doi.org/10.3390/ijerph14101265

Kovochich, M., Liong, M., Parker, J. A., Oh, S. C., Lee, J. P., Xi, L., Kreider, M. L., & Unice, K. M. (2021). Chemical mapping of tire and road wear particles for single particle analysis. *Science of the Total Environment, 757*, 144085. https://doi.org/10.1016/j.scitotenv.2020.144085

Kreider, M. L., Panko, J. M., McAtee, B. L., Sweet, L. I., & Finley, B. L. (2010). Physical and chemical characterization of tire-related particles: Comparison of particles generated using different methodologies. *Science of the Total Environment, 408*, 652–659. https://doi.org/10.1016/j.scitotenv.2009.10.016

Kumata, H., Sanada, Y., Takada, H., & Ueno, T. (2000). Historical trends of N-cyclohexyl-2-benzothiazolamine, 2-(4- morpholinyl)benzothiazole, and other anthropogenic contaminants in the urban reservoir sediment core. *Environmental Science and Technology, 34*, 246–253. https://doi.org/10.1021/es990738k

Kumata, H., Mori, M., Takahashi, S., Takamiya, S., Tsuzuki, M., Uchida, T., & Fujiwara, K. (2011). Evaluation of hydrogenated resin acids as molecular markers for tire-wear debris in urban environments. *Environmental Science and Technology, 45*, 9990–9997. https://doi.org/10.1021/es202156f

Kupiainen, K., Ritola, R., Stojiljkovic, A., Pirjola, L., Malinen, A., & Niemi, J. (2016). Contribution of mineral dust sources to street side ambient and suspension PM10 samples. *Atmospheric Environment, 147*, 178–189. https://doi.org/10.1016/j.atmosenv.2016.09.059

Lundberg, J., Blomqvist, G., Gustafsson, M., Janhäll, S., & Järlskog, I. (2019). Wet dust sampler: A sampling method for road dust quantification and analyses. *Water, Air and Soil Pollution*, *230*. https://doi.org/10.1007/s11270-019-4226-6

Lundberg, J., Gustafsson, M., Janhäll, S., Eriksson, O., Blomqvist, G., & Erlingsson, S. (2020). Temporal variation of road dust load and its size distribution—A comparative study of a porous and a dense pavement. *Water, Air, and Soil Pollution*, *231*. https://doi.org/10.1007/s11270-020-04923-1

Lusher, A. L., Hurley, R., Arp, H. P. H., Booth, A. M., Bråte, I. L. N., Gabrielsen, G. W., Gomiero, A., Gomes, T., Grøsvik, B. E., Green, N., Haave, M., Hallanger, I. G., Halsband, C., Herzke, D., Joner, E. J., Kögel, T., Rakkestad, K., Ranneklev, S. B., Wagner, M., Olsen, M. (2021). Moving forward in microplastic research: A Norwegian perspective. *Environment International*, *157*. https://doi.org/10.1016/j.envint.2021.106794

Ma, Y., Mummullage, S., Wijesiri, B., Egodawatta, P., McGree, J., Ayoko, G. A., & Goonetilleke, A. (2021). Source quantification and risk assessment as a foundation for risk management of metals in urban road deposited solids. *Journal of Hazardous Materials, 408*, 124912. https://doi.org/10.1016/j.jhazmat.2020.124912

Magnusson, K., Winberg von Friesen, L., Söderlund, K., Karlsson, P.-E., & Pinhl Karlsson, G. (2020). Atmosfäriskt nedfall av mikroskräp [Deposition of atmospheric micro-debris]. IVL Svenska Miljöinstitutet, Report C511, 2020. https://www.ivl.se/download/18.5bc68544171830dff503b2/1587372619571/C511.pdf

Müller, A., Österlund, H., Marsalek, J., & Viklander, M. (2020). The pollution conveyed by urban runoff: A review of sources. *Science of the Total Environment, 709*, 136125. https://doi.org/10.1016/j.scitotenv.2019.136125

Nosko, O., & Olofsson, U. (2017). Quantification of ultrafine airborne particulate matter generated by the wear of car brake materials. *Wear, 374–375*, 92–96. https://doi.org/10.1016/j.wear.2017.01.003

Oroumiyeh, F., & Zhu, Y. (2021). Brake and tire particles measured from on-road vehicles: Effects of vehicle mass and braking intensity. *Atmospheric Environment: X*, *12*. https://doi.org/10.1016/j.aeaoa.2021.100121

Panko, J. M., Chu, J. A., Kreider, M. L., McAtee, B. L., & Unice, K. M. (2012). Quantification of tire and road wear particles in the environment. *WIT Transactions on the Built Environment, 128*, 59–70. https://doi.org/10.2495/UT120061

Pant, P., & Harrison, R. M. (2013). Estimation of the contribution of road traffic emissions to particulate matter concentrations from field measurements: A review. *Atmospheric Environment, 77*, 78–97. https://doi.org/10.1016/j.atmosenv.2013.04.028

Parker-Jurd, F. N. F., Napper, I. E., Abbott, G. D., Hann, S., & Thompson, R. C. (2021). Quantifying the release of tyre wear particles to the marine environment via multiple pathways. *Marine Pollution Bulletin, 172*, 112897. https://doi.org/10.1016/j.marpolbul.2021.112897

Piscitello, A., Bianco, C., Casasso, A., & Sethi, R. (2021). Non-exhaust traffic emissions: Sources, characterization, and mitigation measures. *Science of the Total Environment, 766*, 144440. https://doi.org/10.1016/j.scitotenv.2020.144440

Rauert, C., Rødland, E. S., Okoffo, E. D., Reid, M. J., Meland, S., Thomas, K. V. (2021). Challenges with quantifying tire road wear particles: Recognizing the need for further refinement of the ISO technical specification. *Environmental Science & Technology Letters*; https://doi.org/10.1021/acs.estlett.0c00949.

Rausch, J., Jaramillo-Vogel, D., Perseguers, S., Schnidrig, N., Grobéty, B., & Yajan, P. (2022). Automated identification and quantification of tire wear particles (TWP) in airborne dust: SEM/EDX single particle analysis coupled to a machine learning classifier. *Science of the Total Environment, 803*, 149832. https://doi.org/10.1016/j.scitotenv.2021.149832

Rødland, E. S., Samanipour, S., Rauert, C., Okoffo, E. D., Reid, M. J., Heier, L. S., Lind, O. C., Thomas, K. V., & Meland, S. (2022a). A novel method for the quantification of tire and polymer-modified bitumen particles in environmental samples by pyrolysis gas chromatography mass spectroscopy. *Journal of Hazardous Materials, 423*, 127092. https://doi.org/10.1016/j.jhazmat.2021.127092

Rødland, E. S., Lind, O. C., Reid, M. J., Heier, L. S., Okoffo, E. D., Rauert, C., Thomas, K. V., & Meland, S. (2022b). Occurrence of tire and road wear particles in urban and peri-urban snowbanks, and their potential environmental implications. *Science of the Total Environment, 824*, 153785. https://doi.org/10.1016/j.scitotenv.2022.153785

Rogge, W. F., Medeiros, P. M., & Simoneit, B. R. T. (2012). Organic compounds in dust from rural and urban paved and unpaved roads taken during the San Joaquin Valley fugitive dust characterization study. *Environmental Engineering Science, 29*, 1–13. https://doi.org/10.1089/ees.2010.0124

Sethupathi, P. B., Chandradass, J., & Saibalaji, M. A. (2021). Comparative study of disc brake pads sold in Indian market —Impact on safety and environmental aspects. *Environmental Technology & Innovation, 21*, 101245. https://doi.org/10.1016/j.eti.2020.101245

Sommer, F., Dietze, V., Baum, A., Sauer, J., Gilge, S., Maschowski, C., & Gieré, R. (2018). Tire abrasion as a major source of microplastics in the environment. *Aerosol and Air Quality Research, 18*, 2014–2028. https://doi.org/10.4209/aaqr.2018.03.0099

Unice, K. M., Kreider, M. L., & Panko, J. M. (2013). Comparison of tire and road wear particle concentrations in sediment for watersheds in France, Japan, and the United States by quantitative pyrolysis GC/MS analysis. *Environmental Science & Technology, 47*, 8138–8147. https://doi.org/10.1021/es400871j

Verschoor, A., de Poorter, L., Dröge, R., Kuenen, J., & de Valk, E. (2016). Emission of microplastics and potential mitigation measures- Abrasive cleaning agents, paints, and tyre wear. National Institute for Public Health and the Environment. RIVM-Report 2016-0026. https://ia802807.us.archive.org/4/items/blg-777944/blg-777944.pdf

Vogelsang, C., Lusher, A. L., Dadkhah, M. E., Sundvor, I., Umar, M., Ranneklev, S. B., Eidsvoll, D., & Meland, S. (2019). Microplastics in road dust—Characteristics, pathways and measures. Norweigan Institute for Water Research. NIVA-report 7361-2019. https://niva.brage.unit.no/niva-xmlui/handle/11250/2493537

Vojtíšek-Lom, M., Vaculík, M., Pechout, M., Hopan, F., Arul Raj, A. F., Penumarti, S., Horák, J. S., Popovicheva, O., Ondráček, J., & Doušová, B. (2021). Effects of braking conditions on nanoparticle emissions from passenger car friction brakes. *Science of the Total Environment, 788*, 147779. https://doi.org/10.1016/j.scitotenv.2021.147779

Wagner, S., Hüffer, T., Klöckner, P., Wehrhahn, M., Hofmann, T., & Reemtsma, T. (2018). Tire wear particles in the aquatic environment—A review on generation, analysis, occurrence, fate and effects. *Water Research, 139*, 83–100. https://doi.org/10.1016/j.watres.2018.03.051

Wagner, S., Klöckner, P., & Reemtsma, T. (2022). Aging of tire and road wear particles in terrestrial and freshwater environments—A review on processes, testing, analysis and impact. *Chemosphere, 288*, 132467. https://doi.org/10.1016/j.chemosphere.2021.132467

Wahlström, J., Söderberg, A., Olander, L., & Olofsson, U. (2009). A disc brake test stand for measurement of airborne wear particles. *Lubrication Science, 21*, 241–252. https://doi.org/10.1002/ls.87

Williams, R. L., & Cadle, S. H. (1978). Characterization of tire emissions using an indoor test facility. *Rubber Chemistry and Technology, 51*, 7–25. https://doi.org/10.5254/1.3535728

Youn, J.-S., Kim, Y.-M., Siddiqui, M. Z., Watanabe, A., Han, S., Jeong, S., Jung, Y.-W., & Jeon, K.-J. (2021). Quantification of tire wear particles in road dust from industrial and residential areas in Seoul, Korea. *Science of the Total Environment, 784*, 147177. https://doi.org/10.1016/j.scitotenv.2021.147177

Zannoni, D., Valotto, G., Visin, F., & Rampazzo, G. (2016). Sources and distribution of tracer elements in road dust: The Venice mainland case of study. *Journal of Geochemical Exploration, 166*, 64–72. https://doi.org/10.1016/j.gexplo.2016.04.007